Applied Catalysis A, General 657 (2023) 119146

Contents lists available at ScienceDirect

Applied Catalysis A, General

journal homepage: www.elsevier.com/locate/apcata

Adsorption and catalytic ozonation of toluene on Mn/ZSM-5 at low temperature

Bing Zhou [a,b], Quanli Ke [a], Kai Chen [a], Meijun Wen [a], Guokai Cui [a], Ying Zhou [a,*], Zhenyu Gu [b], Xiaole Weng [c], Hanfeng Lu [a,*]

[a] Institute of Catalytic Reaction Engineering, College of Chemical Engineering, Zhejiang University of Technology, Hangzhou 310014, China
[b] Key Laboratory of Environmental Pollution Control Technology Research of Zhejiang Province, Eco-environmental Science Research & Design Institute of Zhejiang Province, Hangzhou 310007, China
[c] Key Laboratory of Environment Remediation and Ecological Health, Ministry of Education, College of Environmental and Resource Sciences, Zhejiang University, Hangzhou 310058, China

ARTICLE INFO

Keywords:
Adsorption
Catalytic ozonation
Toluene
Mn/ZSM-5

ABSTRACT

In this study, a series of Mn/ZSM-5 catalysts with different Mn contents (2, 4, and 6 wt%) were prepared as adsorbents and catalysts. The adsorption of toluene and the regeneration performance of ozone catalytic oxidation at room temperature were investigated. The results showed that the toluene conversion reaches 90 % at 30 ℃ through 4 wt% Mn/ZSM-5 catalytic oxidation. The cycling and ozone utilization rate experiments reflected that after four consecutive adsorption-ozonation cycles, 4 wt% Mn/ZSM-5 still maintained good toluene adsorption capacity. In the regeneration process, the molar ratio of ozone consumption to toluene degradation was about 7.7:1, which was approximate to the theoretical molar ratio (6:1). The product distribution on the surface of ZSM-5 and 4 wt%Mn/ZSM-5 during toluene degradation was determined by GC-MS analysis, and possible mechanism for catalytic oxidation of toluene on the surface of ZSM-5 and 4 wt%Mn/ZSM-5 were proposed.

1. Introduction

Volatile organic compounds (VOCs) are one of the main sources of air pollution and the precursors to the production of ozone (O_3) and fine particles ($PM_{2.5}$) [1–4]. The former will cause the production of photochemical smog while the latter will lead to the production of haze [5–8]. VOCs also seriously endanger people's health and affect their daily life [9–12]. Therefore, scientists are paying more and more attention to the abatement of VOCs. Catalytic oxidation has been widely studied and applied because of its maturity and universal applicability to VOCs. However, catalytic oxidation technology has some problems, such as high reaction temperature and high energy consumption [13–15]. Compared with catalytic oxidation technology, ozone catalytic technology can effectively remove VOCs at room temperature and thus has a better market application prospect [16–20].

At present, the two main process applications of ozone catalytic oxidation technology are (1) the simultaneous ozonization and degradation of VOCs in a reaction tube equipped with catalyst and (2) the consecutive adsorption and then ozonization of VOCs [21–23]. Compared with the former process application, in the consecutive adsorption-ozonization process, ozone does not directly come into contact with VOCs and will not dilute the ozone concentration. The catalyst adsorbs a large amount of organic waste gas, an action that is regarded as a concentration process. In this way, it can realize the interaction between high concentration ozone and high concentration VOCs, improve the reaction rate, realize the stoichiometric reaction between VOC organic molecules and ozone, reduce ozone consumption, and save operation energy consumption [24–27].

Materials with both adsorption and catalytic functions are the key to realizing consecutive adsorption-ozonization function. Studies have shown that Mn-based catalysts have excellent ozone activation ability and catalytic activity [28–32]. In addition, ZSM-5 molecular sieve has a stable structure and large specific surface area, which can provide high specific surface area for the dispersion of metal oxides and the strong adsorption of VOCs and ozone during the reaction [33,34]. At the same time, ZSM-5 molecular sieve has rich Lewis acid sites on its surface, which can promote the activation of ozone adsorbed on its surface to produce reactive oxygen species with even stronger oxidation ability

* Corresponding authors.
E-mail addresses: luhf@zjut.edu.cn, wjfx@zjut.edu.cn (H. Lu).

https://doi.org/10.1016/j.apcata.2023.119146
Received 17 September 2022; Received in revised form 14 January 2023; Accepted 18 March 2023
Available online 20 March 2023

[35–38]. Therefore, using ZSM-5 molecular sieve as carrier to disperse Mn oxide can further improve the activity of the catalyst [39,40].

In this study, Mn/ZSM-5 catalysts with different Mn contents were prepared by using ZSM-5 molecular sieve as carrier and Mn oxide as active component, and their performance differences were discussed. The crystal structure, pore structure, and specific surface area of the catalyst were characterized by XRD, SEM and BET. The recovery of adsorption capacity after multiple adsorption-ozonization cycles was investigated. In addition, the product distribution in the process of toluene degradation was determined by GC-MS analysis, and the possible mechanism of catalytic oxidation of toluene was studied.

2. Materials and methods

2.1. Preparation of catalysts

In this experiment, 4 wt% Mn/ZSM-5 catalyst was taken as an example. ZSM-5 molecular sieves (5 g, Si-to-Al molar ratio: 300) were impregnated in 7.3 mL of manganese nitrate (50 %) solution (the nominal load mass fraction of the Mn element was 4 %, and calculated by the mass of the catalyst carrier, the concentration of the impregnation liquid was 1 mol/L), followed by ultrasound treatment at room temperature for 30 min and impregnation at room temperature for 12 h. The sieves were then dried off at 110 ℃ and roasted at 550 ℃ for 4 h, and thus the catalyst was formed. According to the different amounts of manganese nitrate, the other two catalysts with Mn mass fraction of 2 wt % and 6 wt% were prepared. The preparation method was the same as above.

2.2. Determination of ozone concentration

The ozone concentration was determined by iodometry. For this, 20 mL of KI solution (20%) was weighed and poured into a 250 mL absorption flask. Next, 150 mL of distilled water was added, the sample was taken from the ozonated gas–water vapor mixed outlet after the ozone generator was preheated and stabilized and then pumped into the absorption flask to absorb ozone for 5 min. Timing was started, and the gas throughput was 250 mL. After sampling was stopped, 2.4 mL of sulfuric acid solution (volume ratio of sulfuric acid to water was 1:5) was immediately added to lower the pH value to below 2.0 and then shaken, followed by standing for 5 min. Next, 0.1 mol/L standard sodium thiosulfate solution was used for titration, several drops of starch solution were added when the solution turned pale yellow, and the titration was continued carefully and rapidly until the color disappeared. The use level of standard sodium thiosulfate solution was recorded as 3.12 mL. According to the consumption of sodium thiosulfate solution, the ozone concentration was calculated as 30 g/m^3.

2.3. Catalytic activity measurement

The activity was evaluated in two stages, where the first stage, adsorption stage, proceeded in the reactor of a fixed fluidized bed. The stably structured toluene was taken as the treatment object, brought out through the air bubbling method, and then mixed with the air to simulate the waste gas under practical environmental conditions. In the second stage, catalytic ozonation regeneration, the toluene adsorbed by catalysts was decomposed. On this basis, the activity was evaluated by testing the adsorption capacity of catalysts after each cycle of ozonation regeneration. Highly pure oxygen was used as the gas source in the ozone generator. The ozone concentration was determined through iodometry.

The main experimental conditions and steps were as follows. The air was let out of the steel air cylinder from two ways, where one way of the air was pumped into a bubbling bottle containing toluene via a mass flowmeter for bubbling at 0 ℃, thus generating toluene vapor that was mixed with the air from the other way and diluted to obtain the required toluene inlet concentration (C_0). After dilution, the toluene concentration was 9000 mg/m^3 and the total gas flow was 167 mL/min. Subsequently, the waste gas was continuously pumped into a U-shaped reaction tube containing 1 g of the catalyst. This process was stopped (i.e., the adsorption step was completed) when the outlet concentration of toluene was equivalent to the inlet concentration ($C_i = C_0$), that is, after the catalyst reached saturated adsorption. Since the adsorption was greatly influenced by the temperature, the adsorption temperature was controlled at 30 ℃ through a thermostat water batch in an effort to avoid experimental errors. Afterwards, the humidified ozonated gas was pumped into the U-shaped reaction tube for the oxidation reaction for 3 h and then the ozonation regeneration ended. The flow rate of humidified ozonated gas was 50 mL/min, concentration was 30 g/m^3, and RH was 100 %. The inlet and outlet concentrations of toluene in the adsorption process and the outlet concentration of toluene in the regeneration process were determined via Agilent 6890 gas chromatograph equipped with an FID detector. The inlet and outlet concentrations of ozone were regulated by changing the discharging current of the ozone generator and measured through iodometry.

The toluene adsorption capacity of the catalyst per unit mass is calculated through the following Eq. (1):

$$q = \frac{F \times C_0 \times 10^{-6}}{W}\left[t_s - \int_0^{t_s} \frac{C_i}{C_0} dt\right] \quad (1)$$

where q is the saturated adsorption capacity, mg/g; t_s is the time when adsorption equilibrium is reached, min; F is the total gas flow, 167 mL/min; W is the mass of the catalyst, g; C_0 is the inlet mass concentration (i.e., the initial mass concentration) of the adsorbed gas, mg/m^3; and C_i is the outlet mass concentration of the adsorbed gas, mg/m^3.

The ozone consumption needed by per unit mass of the catalyst to adsorb toluene is calculated through the following Eq. (2):

$$q_{O3} = \frac{F \times C_0 \times 10^{-6}}{W}\int_{t_A}^{t_B}\left(1 - \frac{C_i}{C_0}\right) dt \quad (2)$$

where q_{O3} stands for the ozone consumption, g/g; F is the total gas flow of ozone, 50 mL/min; W is the mass of the catalyst, g; t_A and t_B represent the starting time and ending time of the regeneration experiment, respectively, min; and C_0 denotes the inlet concentration of ozone, namely, the initial concentration, g/m^3.

In the ozonation process, the toluene desorption of per unit mass of catalyst is calculated through the following Eq. (3):

$$q = \frac{F \times 10^{-6}}{W}\int_{t_A}^{t_B} C_i dt \quad (3)$$

where q is the toluene desorption, mg/g; F is the total gas flow of ozone, 50 mL/min; W is the mass of the catalyst, g; t_A and t_B represent the starting time and ending time of the regeneration experiment, respectively, min; and C_i denotes the outlet mass concentration of toluene, mg/m^3.

2.4. Characterization of catalysts

The XRD characterization was implemented on an X′Pert PRO X-ray diffractometer of the Dutch PANalytical Corporation. In this process, Ni filtering was performed; the Kα ray ($\lambda = 0.1541$ nm) generated by the Cu target was employed to stimulate the sample to generate diffraction; the tube voltage and current were 40 kV and 40 mA, respectively; the scanning range was 10–80°; and the scanning speed was 0.02°s^{-1}. Surface morphologies of the sample were characterized using a scanning electron microscope (S-4700, Japanese Hitachi Company) with the emission voltage of 29.0 kV, and metal spraying was implemented for the sample before the test. The textural properties of the catalysts, including specific surface area, pore volume, pore diameter, and total porosity, were analyzed on the 3Flex Surface Property Analyzer

produced by Micromeritics Company and measured using − 196 ℃ nitrogen adsorption/desorption isotherms. Before the experiment, degasification treatment was conducted in a vacuum at 150 ℃ for 8 h, and the specific surface area of each sample was calculated through the BET model.

3. Results and discussion

3.1. Toluene removal by the adsorption–ozonization process

The time-dependent changes of toluene concentration in one adsorption-ozonation regeneration cycle of the four catalysts are shown in Fig. 1, where all four fresh catalysts are demonstrated to have reached saturated adsorption ($C_i = C_0$) after 162 min. The saturated adsorption capacity is displayed in Fig. 2. Fig. 2 shows that with the increase of Mn loading, the toluene adsorption capacity of fresh catalysts was gradually reduced, which could be explained by the reduction of their specific surface area and pore volume. In this case, the pumping of organic waste gas was stopped, and the catalytic ozonation regeneration of the adsorbed toluene was implemented. When the catalytic ozonization regeneration steps started, a very high peak of toluene concentration (Fig. 1) was detected through the chromatographic detection, indicating that one part of the toluene adsorbed by catalysts was desorbed. When the catalytic ozonation regeneration steps were completed, the organic waste gas flow was fed into the catalyst bed once again under the same conditions as the first adsorption step. It could be observed from Fig. 1 that the adsorption capacity of Mn/ZSM-5 after the adsorption-ozonation regeneration cycles obviously recovered better than that of ZSM-5 and the toluene desorption capacity accounted for a very small proportion. The specific values could be clearly seen from Fig. 2. Through the toluene adsorption capacity of the four catalysts as well as the proportions of toluene desorption capacity and degradation before and after the reaction, the following conclusions could be drawn: catalytic activity was enhanced after ZSM-5 carried Mn active components, and 4 wt% Mn/ZSM-5 presented the highest recovery degree of toluene adsorption capacity and the best toluene degradation performance.

The ozone escape rate in the regeneration process could be calculated according to the time-dependent changes of outlet ozone concentration versus the inlet one (C_i/C_0). As shown in Fig. 3, the ozone escape rates of the four catalysts were sorted as ZSM-5 (17.3 %)> 2 wt%Mn/ZSM-5 (7.13 %)> 6 wt%Mn/ZSM-5 (5.40 %)> 4 wt%Mn/ZSM-5 (5.01 %). When the ZSM-5 zeolites were loaded with the active components of Mn oxides, the activation performance of ozone was considerably improved because the Mn oxides were the catalyst reaching the highest ozone activation efficiency among gaseous media. Besides, there were rich Lewis acid sites on the surface of the ZSM-5 molecular sieves, which facilitated the activation of the ozone adsorbed on the surface to generate reactive oxygen species with stronger oxidation capacity.

The ozone consumption to toluene degradation ratios of the four catalysts are reflected in Fig. 4. This ratio could serve as a measure of

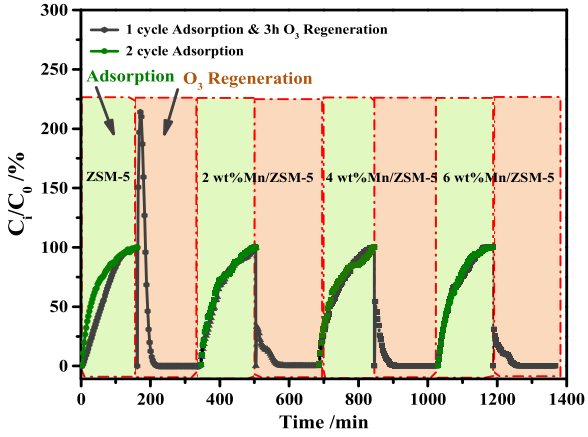

Fig. 1. Variation of the ratio of the concentration of toluene at the outlet and inlet (C_i/C_0) of the reactor with time.

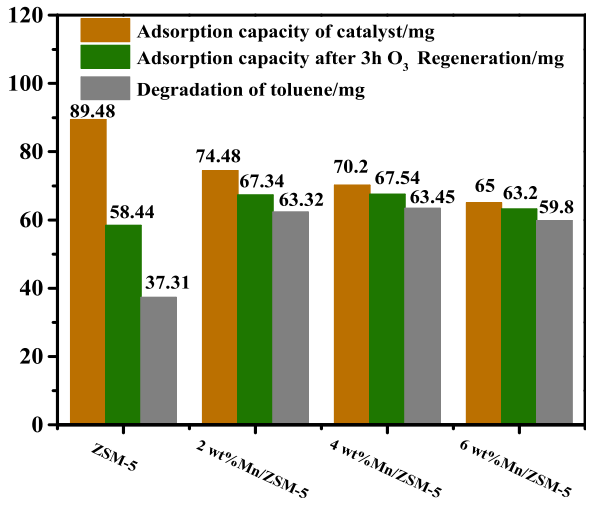

Fig. 2. The degradation capacity of toluene and the adsorption capacity before and after the reaction of the four catalysts.

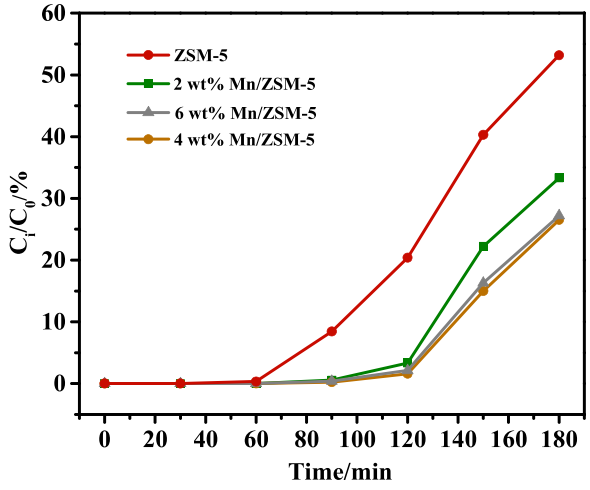

Fig. 3. Variation of the ratio of the concentration of O_3 at the outlet and inlet (C_i/C_0) of the reactor with time.

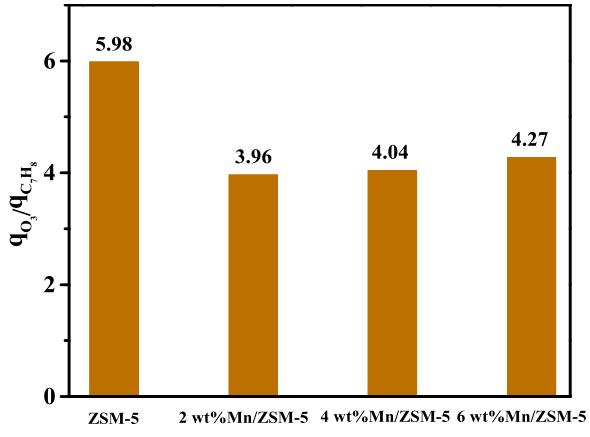

Fig. 4. Ratio of ozone consumption to toluene degradation of the four catalysts.

ozone utilization rate. Next, the theoretical amount of ozone needed by the catalyst reduction is calculated based on the toluene–ozone reaction Eq. (4):

$$C_7H_8 + 6\ O_3 \rightarrow 7CO_2 + 4\ H_2O \quad (4)$$

On the precondition of permineralization, the theoretical molar ratio of ozone to toluene was 6:1, which translates to a mass ratio of approximately 3.13:1. Fig. 4 shows that the ratios of ozone consumption versus toluene degradation on Mn/ZSM-5 catalysts with different Mn contents (2, 4, and 6 wt%) were mostly close to 3.13:1, manifesting that the adsorption-ozonization regeneration process was very energy-saving and efficient.

3.2. Catalyst characterization

Given the relatively good catalytic toluene oxidation properties and low ozone escape rate of 4 wt%Mn/ZSM-5, a further characterization analysis was performed for this catalyst. First, the phase structures of ZSM-5 and 4 wt%Mn/ZSM-5 were analyzed; their XRD graphs are shown in Fig. 5. The results show that both ZSM-5 and 4 wt%Mn/ZSM-5 had high-intensity triple characteristic peaks at the same position ($2\theta = 23–25^\circ$). Clearly, both samples were of typical MFI structures. The diffractogram of 4 wt%Mn/ZSM-5 was very similar to that of ZSM-5, indicating that even after ZSM-5 molecular sieves carried Mn active components, the catalyst still kept its original morphological structure. However, no obvious MnO_x characteristic peak was observed on the diffraction pattern of 4 wt%Mn/ZSM-5, which might be related to the low Mn content and its uniform dispersion on ZSM-5.

Next, the surface morphologies of 4 wt%Mn/ZSM-5 were analyzed, and it was found that the morphologies were not evidently changed before and after loading. This was possibly because the Mn content was low, leading to the failure of MnO_x to crystallize and grow into specific morphologies on the ZSM-5 surface. Therefore, mapping characterization analysis of 4 wt%Mn/ZSM-5 was also conducted to explore the elements contained in the prepared 4 wt%Mn/ZSM-5 catalyst and their dispersion status. The results are exhibited in Fig. 6. Mn, Al, Si, and O elements were observed and uniformly dispersed, thus verifying the effective loading of Mn.

As shown in Fig. 7, both ZSM-5 and 4 wt% Mn/ZSM catalysts had hysteresis loops at $P/P_0 = 0.4–1.0$, indicating that mesoporous structures existed both before and after the loading of Mn active components on ZSM-5 molecular sieves.

The specific surface area, average pore diameter, and total pore volume of prepared samples are listed in Table 1. The specific surface area of ZSM-5 reached 315 m^2/g, which was very important for the high dispersity of MnO_x. The specific surface area of 4 wt%Mn/ZSM-5 was smaller than that of ZSM-5, and it was gradually reduced with the increase in Mn load along with its pore volume. This was probably because the introduced MnO_x occupied some pores of ZSM-5, giving rise to the pore blockage. In addition, the four catalysts were only slightly different in pore size distribution (~2.85 nm), manifesting that the introduced MnO_x only changed the framework loose degree of ZSM-5 but did not destroy its overall structure.

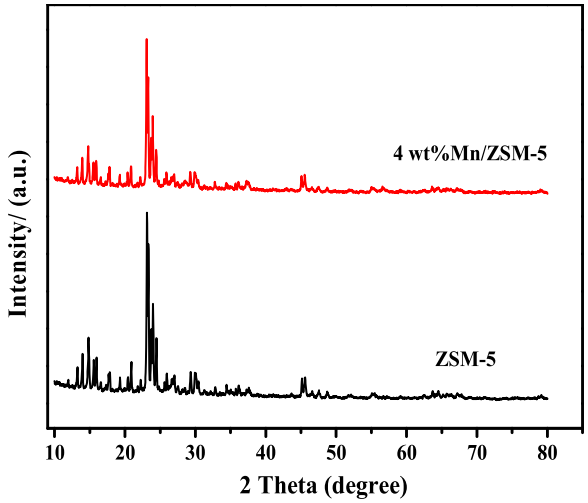

Fig. 5. XRD patterns of ZSM-5 and 4 wt%Mn/ZSM-5.

3.3. Continuous cycling experiment on adsorption–ozonization regeneration

The four-cycle adsorption-ozonation experimental results of 4 wt% Mn/ZSM-5 under the same operating conditions are depicted in Figs. 8 and 9. It could be seen from Fig. 8 that after each adsorption-ozonization cycle, the breakthrough adsorption curves of toluene presented the same appearance, and the saturated adsorption time was stabilized at around 162 min. A comparison of the toluene adsorption rates before and after ozonization indicated that the adsorption capacity of the catalysts was effectively recovered. Likewise, Fig. 8 shows that with the increase of adsorption-ozonation cycles, the outlet toluene concentration of the reaction tube was slightly reduced, possibly because of the ozone regeneration process where the byproducts generated by the non-permineralization of partial toluene covered some active sites, leading to the reduction of toluene desorption.

The recovery of adsorption capacity after each adsorption-ozonation cycle is calculated through Eq. (5), and the results are listed in Table 2:

$$RE = \frac{q}{q_1} \times 100\% \quad (5)$$

where *RE*(%) denotes the recovery rate of adsorption capacity; q is the adsorption capacity after each adsorption-ozonation cycle, mg/g; and q_1 is the adsorption capacity before reaction, mg/g. The recovery rate of adsorption capacity achieved by 4 wt%Mn/ZSM-5 was 77.2–96.2%. The recovery status of adsorption capacity was not only associated with the site regeneration but also with the analytical desorption of partial toluene in the ozonation process.

3.4. GC-MS analysis of intermediate products in toluene degradation process

To determine the main intermediate products on the surface of ZSM-5 and 4 wt%Mn/ZSM-5 in the ozone regeneration process, the products on the catalyst surface were determined via GC-MS, as shown in Figs. 10 and 11, and the corresponding substances are listed in Tables 3 and 4. From Fig. 10 and Table 3, the main products on the ZSM-5 surface are shown to include ethylbenzene, p-xylene, o-xylene, benzaldehyde, benzyl alcohol, benzyl formate, 2-acetoxyacetophenone, benzoic acid, and 2,5-dimethyl benzaldehyde. Noteworthy is that toluene did not exist in the products, which might be attributed to the catalytic reforming of toluene on the ZSM-5 surface. As revealed by Fig. 11 and Table 4, the main products on the surface of 4 wt%Mn/ZSM-5 were ethylbenzene, p-xylene, o-xylene, benzaldehyde, benzyl alcohol, benzyl formate, and benzoic acid. Different from the products on the ZSM-5 surface, the product content on the surface of 4 wt%Mn/ZSM-5 was evidently reduced without the byproducts formed by deep oxidation.

3.5. Deduction of catalytic toluene degradation path

Catalytic ozonation of VOCs is regarded as a heterogeneous reaction that proceeds on the catalyst surface. The reaction follows the Langmuir Hinshelwood (L-H) and/or Mars-van-Krevelen (MvK) mechanisms [18]. According to the above mechanisms, there are two high-activity intermediate products in the ozone regeneration process: O* , which is

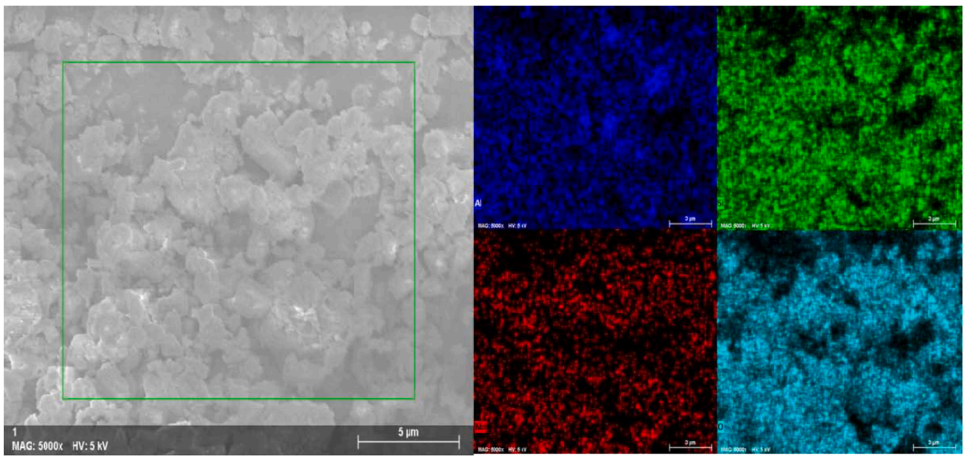

Fig. 6. Mapping images of 4 wt%Mn/ZSM-5.

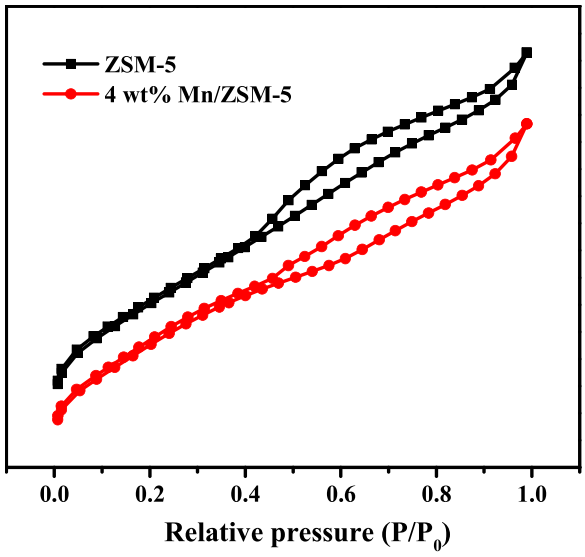

Fig. 7. N_2 adsorption-desorption isotherms of ZSM-5 and 4 wt%Mn/ZSM-5.

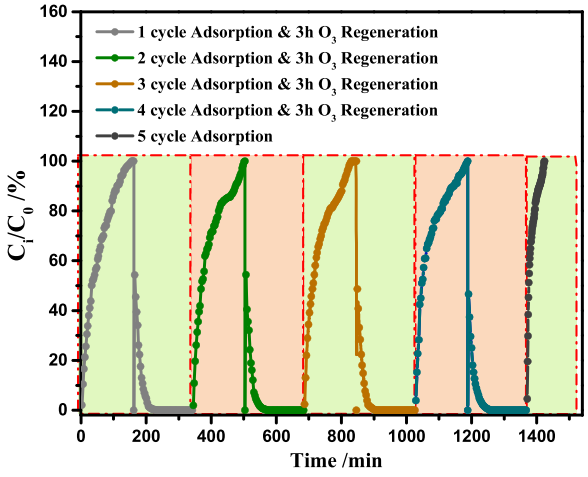

Fig. 8. Time-dependant variation of the ratio between the outlet and inlet toluene concentrations (C_i/C_0) in the reactor during four consecutive adsorption–ozonation cycles on 4 wt%Mn/ZSM-5.

Table 1
Pore structure parameters and S_{BET} of four catalysts.

Sample	S_{BET} (m^2/g)	V_{pore} (cm^3/g)	D_{pore} (nm)
ZSM-5	315	0.23	2.88
2 wt%Mn/ZSM-5	301	0.21	2.85
4 wt%Mn/ZSM-5	292	0.21	2.84
6 wt%Mn/ZSM-5	285	0.20	2.84

generated by the reaction between the adsorbed O_3 with the active Lewis acid sites on the catalyst surface, and OH* , which is generated by the interaction between O_3 and the water vapor existing in the reaction gas. Previous studies have shown that among the toluene molecules, the C–H bond energy of methyl, C–C bond energy connecting methyl and benzene ring, and C–H bond energy and C–C bond energy of benzene ring were 3.7, 4.14, 4.19, and 5.0–5.5 eV, respectively [35]. According to the GC-MS determination results, the possible paths for catalytic toluene oxidation on the surface of ZSM-5 and 4 wt%Mn/ZSM-5 were proposed from the angle of chemical bond energy, as shown in Figs. 12 and 13.

From the perspective of chemical bond energy, among all the chemical bonds of toluene, $C_6H_5CH_2$–H was a chemical bond that could be easily oxidized the most. The formation paths of $C_6H_5CH_2$–OH,

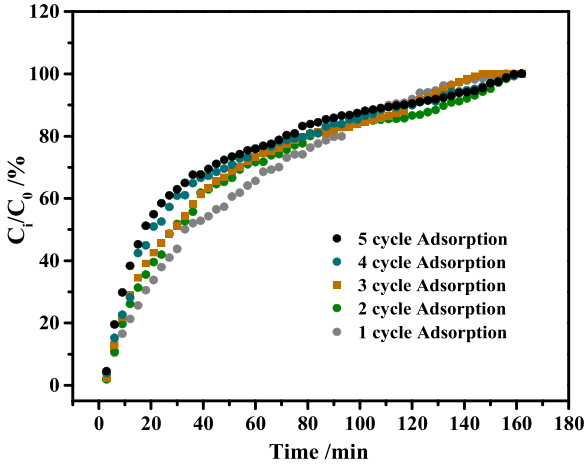

Fig. 9. Comparison of toluene adsorption breakthrough curves after each cycle of adsorption–ozonization.

$C_6H_5CH{=}O$, and C_6H_5COOH could be inferred by combining the GC-MS results. As indicated by the reaction path a in Figs. 12 and 13, toluene (C_6H_5–CH_3) was first oxidized into $C_6H_5CH_2$–OH by the high-activity

Table 2
Saturated adsorption capacity and recovery rate (RE%) of toluene after each cycle of adsorption–ozonization.

Cycles	q (mg/g)	RE (%)
1st cycle	70.2	-
2nd cycle	67.54	96.2
3rd cycle	62.56	89.1
4th cycle	58.6	83.5
5th cycle	54.2	77.2

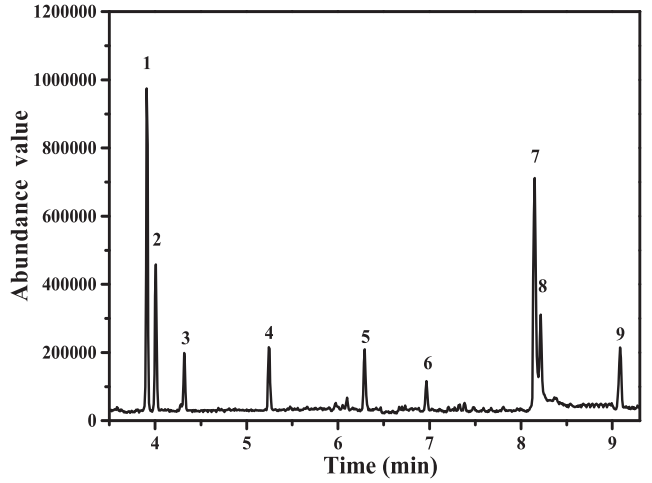

Fig. 10. GC-MS measurements of the products on the surface of ZSM-5 during toluene degradation process.

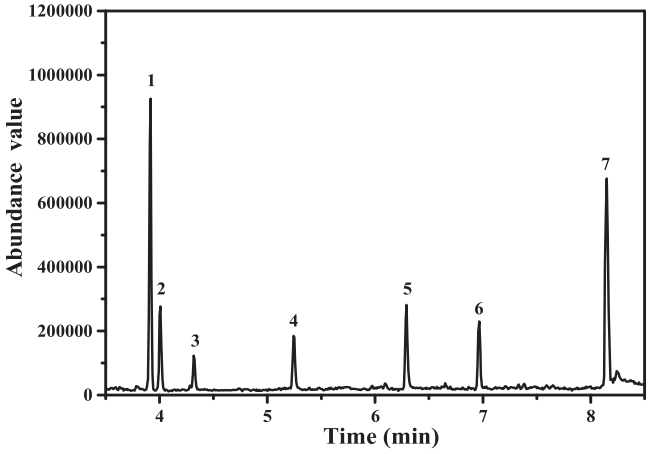

Fig. 11. GC-MS measurements of the products on the surface of 4 wt%Mn/ZSM-5 during toluene degradation process.

intermediate product OH* or O*, and $C_6H_5CH_2$–OH was then oxidized into C_6H_5CH=O, which was further oxidized into C_6H_5COOH. On this basis, benzyl formate was generated by the esterification reaction between C_6H_5CH=O and HCOOH, as indicated by the reaction path b in Fig. 12. C_6H_5–CH_3 was the bond that could be most easily oxidized just second to $C_6H_5CH_2$–H. The formation paths of p-xylene, n-xylene, and m-xylene could be inferred by combining the GC-MS results. The free -CH_3 had four reaction paths. First, it could be continuously oxidized to generate CO_2 and H_2O. Second, it could bind to toluene to generate p-xylene, n-xylene, and m-xylene, as reflected by the reaction path c in Fig. 12. Third, it could bind to toluene to generate 1,2,4-tritoluene and be further oxidized into 2,5-dimethyl benzaldehyde by OH* or O*, as indicated by the reaction path d in Fig. 12. Fourth, it could bind to

Table 3
Main products on the surface of ZSM-5.

Number	Peak time (min)	Chemical compound	Molecular formula
1	3.917	ethylbenzene	C_8H_{10}
2	4.017	P-xylene	C_8H_{10}
		m-xylene	C_8H_{10}
3	4.314	m-xylene	C_8H_{10}
		P-xylene	C_8H_{10}
		O-xylene	C_8H_{10}
4	5.250	Benzaldehyde	C_7H_6O
5	6.300	Benzyl alcohol	C_7H_8O
6	6.975	Benzyl formate	$C_8H_8O_2$
7	8.217	Benzoic acid	$C_7H_6O_2$
8	8.223	Phenacyl acetate	$C_{10}H_{10}O_3$
9	9.103	2,5-Dimethylbenzaldehyde	$C_9H_{10}O$

Table 4
Main products on the surface of 4 wt%Mn/ZSM-5.

Number	Peak time (min)	Chemical compound	Molecular formula
1	3.917	ethylbenzene	C_8H_{10}
2	4.017	P-xylene	C_8H_{10}
		m-xylene	C_8H_{10}
3	4.314	m-xylene	C_8H_{10}
		P-xylene	C_8H_{10}
		O-xylene	C_8H_{10}
4	5.250	Benzaldehyde	C_7H_6O
5	6.300	Benzyl alcohol	C_7H_8O
6	6.975	Benzyl formate	$C_8H_8O_2$
7	8.217	Benzoic acid	$C_7H_6O_2$

HCOOH to generate CH_3COOH, react with benzyl alcohol, or be further oxidized into 2-acetoxyacetophenone by OH* or O*, as revealed by the reaction path e in Fig. 12. According to the relative intensity of peaks in Figs. 10 and 11, it could be inferred that apart from the relatively high-intensity ethylbenzene peak formed by the catalytic reforming of toluene on the surface of ZSM-5, C_6H_5COOH plays a dominant role among the numerous byproducts. This is mainly because benzoic acid, which is relatively stable, cannot be easily oxidatively decomposed. Therefore, the main way of catalytic degradation of toluene is:

$$C_6H_5\text{-}CH_3 \rightarrow C_6H_5CH_2\text{-}OH \rightarrow C_6H_5CH{=}O \rightarrow C_6H_5COOH\cdot$$

4. Conclusion

In this study, ZSM-5 molecular sieve was used as the carrier and Mn oxides as the active components to prepare Mn/ZSM-5 catalysts with different Mn contents (2, 4, and 6 wt%), coupled with the adsorption–ozonation process to purify toluene. In this process, the toluene conversion reached 90 % at 30 ℃ through 4 wt%Mn/ZSM-5 catalytic oxidation. Moreover, the recovery rate of toluene adsorption capacity, catalytic activity, and ozone utilization rate of the catalysts were investigated. Experimental results showed that after one adsorption-ozonation cycle, 4 wt%Mn/ZSM-5 demonstrated the highest toluene adsorption capacity and degradation (67.54 and 63.45 mg/g, respectively), along with the lowest ozone escape rate (5.01 %) and the best degradation performance. Subject to four consecutive adsorption–ozonization cycles, 4 wt%Mn/ZSM-5 still retained good adsorptive properties (the recovery rate of adsorption capacity was 77.2–96.2 %). In the regeneration process, the molar ratio of ozone consumption versus toluene degradation was about 7.7:1, which was approximate to the theoretical molar ratio (6:1). Hence, it is very reasonable and effective to purify toluene by combining Mn/ZSM-5, as the adsorbent/catalyst, with the adsorption–ozonization process.

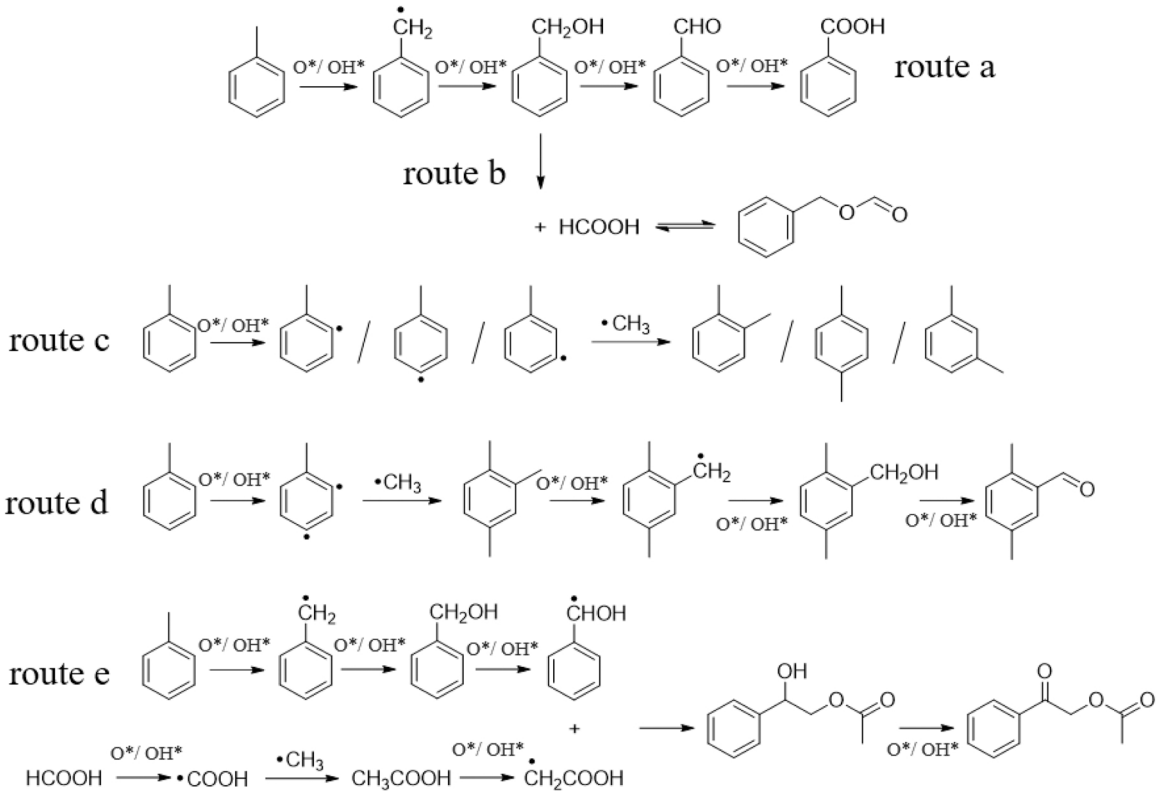

Fig. 12. Proposed catalytic degradation pathways of toluene in the presence of O_3 by ZSM-5.

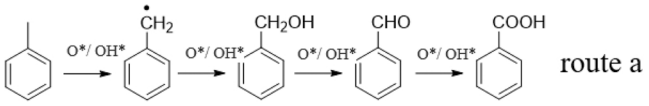

Fig. 13. Proposed catalytic degradation pathways of toluene in the presence of O_3 by 4 wt%Mn/ZSM-5.

CRediT authorship contribution statement

Author 1 (First Author): Conceptualization, Methodology, Investigation, Data Curation, Formal Analysis, Writing-Original Draft, **Author 2:** Data Curation, Writing-Original Draft, **Author 3:** Visualization, Investigation, **Author 4:** Resources, Visualization, **Author 5:** Software, Validation, Funding Acquisition, **Author 6(Corresponding Author):** Visualization, Writing-Review & Editing, **Author 7:** Validation, Investigation, Funding Acquisition; **Author 8:** Supervision, Validation; **Author 9 (Corresponding Author):** Conceptualization, Funding Acquisition, Resources, Supervision, Writing-Review & Editing.

Declaration of Competing Interest

The authors declare that they have no known competing financial interests or personal relationships that could have appeared to influence the work reported in this paper.

Data availability

I have shared the link to my date/code at the Attach File step.

Acknowledgments

This work was supported by the National Natural Science Foundation of China (22078294, 21922607), Scientific Research Fund of Zhejiang Provincial Education Department (Y202043197), the Natural Science Foundation of Zhejiang Province (LZ21E080001, LGF20E080018) and the Key Laboratory of Environmental Pollution Control Technology Research of Zhejiang Province (2021ZEKL04).

References

[1] X.H. Cao, J.C. Lu, X.Q. Zheng, D.D. He, W.J. Zhu, Y.T. Zhao, W.J. Zhang, R. Tian, Y. M. Luo, Regulation of the reaction pathway to design the high sulfur/coke-tolerant Ce-based catalysts for decomposing sulfur-containing VOCs, Chem. Eng. J. 429 (2022), 132473, https://doi.org/10.1016/j.cej.2021.132473.

[2] L. Chen, Y.F. Liao, Y. Chen, J.N. Wu, X.Q. Ma, Performance of Ce-modified V-W-Ti type catalyst on simultaneous control of NO and typical VOCs, Fuel Process Technol. 207 (2020), 106483, https://doi.org/10.1016/j.fuproc.2020.106483.

[3] K.B. Kim, S.Y. Jeong, T.H. Kim, Y.C. Kang, J.H. Lee, Methylbenzene sensors using Ti-doped NiO multiroom spheres: Versatile tunability on selectivity, response, sensitivity, and detection limit, Sens. Actuators B-Chem. 308 (2020), 127730, https://doi.org/10.1016/j.snb.2020.127730.

[4] J.L. Wang, X.L. Guo, Y.J. Shi, R.X. Zhou, Synergistic effect of Pt nanoparticles and micro-mesoporous ZSM-5 in VOCs low-temperature removal, J. Environ. Sci. 107 (2021) 87–97, https://doi.org/10.1016/j.jes.2021.01.033.

[5] X.Y. Yang, B. Yuan, Z. Peng, Y.W. Peng, C.H. Wu, S.X. Yang, J. Li, M. Shao, Inter-comparisons of VOC oxidation mechanisms based on box model: A focus on OH reactivity, J. Environ. Sci. 114 (2022) 286–296, https://doi.org/10.1016/j.jes.2021.09.002.

[6] H.Y. Zhao, H. Wang, Z.P. Qu, Synergistic effects in Mn-Co mixed oxide supported on cordierite honeycomb for catalytic deep oxidation of VOCs, J. Environ. Sci. 112 (2022) 231–243, https://doi.org/10.1016/j.jes.2021.05.003.

[7] Z. Shayegan, F. Haghighat, C.S. Lee, Surface fluorinated Ce-doped TiO_2 nanostructure photocatalyst: A trap and remove strategy to enhance the VOC removal from indoor air environment, Chem. Eng. J. 401 (2020), 125932, https://doi.org/10.1016/j.cej.2020.125932.

[8] M. Zang, C.C. Zhao, Y.Q. Wang, S.Q. Chen, A review of recent advances in catalytic combustion of VOCs on perovskite-type catalysts, J. Saudi Chem. Soc. 23 (2019) 645–654, https://doi.org/10.1016/j.jscs.2019.01.004.

[9] Z. Abbasi, M. Haghighi, E. Fatehifar, S. Saedy, Synthesis and physicochemical characterizations of nanostructured Pt/Al_2O_3–CeO_2 catalysts for total oxidation of VOCs, J. Hazard. Mater. 186 (2011) 1445–1454, https://doi.org/10.1016/j.jhazmat.2010.12.034.

[10] H.Y. Chen, Z.H. You, X. Wang, Q.M. Qiu, Y.B. Ying, Y.X. Wang, An artificial olfactory sensor based on flexible metal–organic frameworks for sensing VOCs, Chem. Eng. J. 446 (2022), 137098, https://doi.org/10.1016/j.cej.2022.137098.

[11] Z.X. Cuo, Y.Z. Deng, W.H. Li, S.P. Peng, F. Zhao, H.D. Liu, Y.F. Chen, Monolithic Mn/Ce-based catalyst of fibrous ceramic membrane for complete oxidation of benzene. Appl. Surf. Sci. 456 (2018) 594–601, https://doi.org/10.1016/j.apsusc.2018.06.207.
[12] B.J. Dou, R.Z. Zhao, N.N. Yan, C.C. Zhao, Q.L. Hao, K.S. Hui, K.N. Hui, A facilitated synthesis of hierarchically porous Cu–Ce–Zr catalyst using bacterial cellulose for VOCs oxidation, Mater. Chem. Phys. 237 (2019), 121852, https://doi.org/10.1016/j.matchemphys.2019.121852.
[13] T.Y. Cheng, J.J. Li, X.W. Ma, L. Zhou, H. Wu, L.J. Yang, Alkylation modified pistachio shell-based biochar to promote the adsorption of VOCs in high humidity environment, Environ. Pollut. 295 (2022), 118714, https://doi.org/10.1016/j.envpol.2021.118714.
[14] Y. Wang, D.Y. Yang, S.Z. Li, M.Q. Chen, L.M. Guo, J. Zhou, Ru/hierarchical HZSM-5 zeolite as efficient bi-functional adsorbent/catalyst for bulky aromatic VOCs elimination, Microporous Mesoporous Mater. 258 (2018) 17–25, https://doi.org/10.1016/j.micromeso.2017.08.052.
[15] G.X. Zhu, J.G. Zhu, W.J. Jiang, Surface oxygen vacancy induced α-MnO_2 nanofiber for highly efficient ozone elimination, Appl. Catal. B 209 (2017) 729–737, https://doi.org/10.1016/j.apcatb.2017.02.068.
[16] S.F. Cheng, F. Lu, P. Peng, J. Zheng, Emission characteristics and control scenario analysis of VOCs from heavy-duty diesel trucks, J. Environ. Manag. 293 (2021), 112915, https://doi.org/10.1016/j.jenvman.2021.112915.
[17] F.W. Lin, Z.M. Zhang, N. Li, B.B. Yan, C. He, Z.P. Hao, G.Y. Chen, How to achieve complete elimination of Cl-VOCs: A critical review on byproducts formation and inhibition strategies during catalytic oxidation, Chem. Eng. J. 404 (2021), 126534, https://doi.org/10.1016/j.cej.2020.126534.
[18] B.Y. Liu, J. Ji, B.G. Zhang, W.J. Huang, Y.L. Gan, D.Y.C. Leung, H.B. Huang, Catalytic ozonation of VOCs at low temperature: A comprehensive review, J. Hazard. Mater. 422 (2022), 126847, https://doi.org/10.1016/j.jhazmat.2021.126847.
[19] Y.J. Shi, J.L. Wang, R.X. Zhou, Pt-support interaction and nanoparticle size effect in Pt/CeO_2–TiO_2 catalysts for low temperature VOCs removal, Chemosphere 265 (2021), 129127, https://doi.org/10.1016/j.chemosphere.2020.129127.
[20] S.S. Zhang, W.H. Pu, A. Chen, Y. Xu, Y.Y. Wang, C.Z. Yang, J.Y. Gong, Oxygen vacancies enhanced photocatalytic activity towards VOCs oxidation over Pt deposited Bi_2WO_6 under visible light, J. Hazard. Mater. 384 (2020), 121478, https://doi.org/10.1016/j.jhazmat.2019.121478.
[21] Y.J. Shi, Z.M. Li, J.L. Wang, R.X. Zhou, Synergistic effect of Pt/Ce and USY zeolite in Pt-based catalysts with high activity for VOCs degradation, Appl. Catal. B 286 (2021), 119936, https://doi.org/10.1016/j.apcatb.2021.119936.
[22] P. Yang, S.K. Fan, Z.Y. Chen, G.F. Bao, S.F. Zuo, C.Z. Qi, Synthesis of Nb_2O_5 based solid superacid materials for catalytic combustion of chlorinated VOCs, Appl. Catal. B 239 (2018) 114–124, https://doi.org/10.1016/j.apcatb.2018.07.061.
[23] H. Zaitan, M.H. Manero, H. Valdés, Application of high silica zeolite ZSM-5 in a hybrid treatment process based on sequential adsorption and ozonation for VOCs elimination, J. Environ. Sci. 41 (2016) 59–68, https://doi.org/10.1016/j.jes.2015.05.021.
[24] V. Chaudhary, S.P. Nehra, Pt-sensitized MoO_3/mpg-CN mesoporous nanohybrid: A highly sensitive VOC sensor, Microporous Mesoporous Mater. 315 (2021), 110906, https://doi.org/10.1016/j.micromeso.2021.110906.
[25] S.C. Lu, Q.L. Liu, R. Han, M. Guo, J.Q. Shi, C.F. Song, N. Ji, X.B. Lu, D.G. Ma, Potential applications of porous organic polymers as adsorbent for the adsorption of volatile organic compounds, J. Environ. Sci. 105 (2021) 184–203, https://doi.org/10.1016/j.jes.2021.01.007.
[26] J.H. Park, J.M. Kim, J. Jurng, G.N. Bae, S.H. Park, S.C. Kim, J.K. Keon, Y.K. Park, Catalytic oxidation of benzene with ozone over Mn/KIT-6, J. Nanosci. Nanotechnol. 13 (2013) 423–426, https://doi.org/10.1166/jnn.2013.6952.
[27] M. Zhang, S.C. Cai, J.J. Li, E.A. Elimian, J. Chen, H.P. Jia, Ternary multifunctional catalysts of polymeric carbon nitride coupled with Pt-embedded transition metal oxide to enhance light-driven photothermal catalytic degradation of VOCs, J. Hazard. Mater. 412 (2021), 125266, https://doi.org/10.1016/j.jhazmat.2021.125266.
[28] E. Hisahiro, M. Nanako, T. Yasutake, Effect of catalyst composition and preparation conditions on catalytic properties of unsupported manganese oxides for benzene oxidation with ozone, Appl. Catal. B. 142–143 (2013) 406–413, https://doi.org/10.1016/j.apcatb.2013.05.041.
[29] B.H. Song, C.T. Li, X.Y. Du, S.H. Li, Y.D. Zhang, Y. Lyu, Q.H. Zhou, Superior performance of Cu-Ce binary oxides for toluene catalytic oxidation: Cu-Ce synergistic effect and reaction pathways, Fuel 306 (2021), 121654, https://doi.org/10.1016/j.fuel.2021.121654.
[30] P. Stefanov, S. Todorova, A. Naydenov, B. Tzaneva, H. Kolev, G. Atanasova, D. Stoyanova, Y. Karakirova, K. Aleksieva, On the development of active and stable Pd-Co/γ-Al_2O_3 catalyst for complete oxidation of methane, Chem. Eng. J. 266 (2015) 329–338, https://doi.org/10.1016/j.cej.2014.12.099.
[31] H.L. Xiao, J.L. Wu, X.Q. Wang, J.L. Wang, S.P. Mo, M.L. Fu, L.M. Chen, D.Q. Ye, Ozone-enhanced deep catalytic oxidation of toluene over a platinum-ceria-supported BEA zeolite catalyst, Mol. Catal. 460 (2018) 7–15, https://doi.org/10.1016/j.mcat.2018.09.005.
[32] Z.M. Zhang, L. Xiang, F.W. Lin, Z. Wang, B.B. Yan, G.Y. Chen, Catalytic deep degradation of Cl-VOCs with the assistance of ozone at low temperature over MnO_2 catalysts, Chem. Eng. J. 426 (2021), 130814, https://doi.org/10.1016/j.cej.2021.130814.
[33] R. Ebrahim, S. Jafar, Low temperature oxidation of toluene by ozone over MnO_x/γ-alumina and MnO_x/MCM-41 catalysts, Chem. Eng. J. 198–199 (2012) 482–490, https://doi.org/10.1016/j. cej.2012.06.016.
[34] R.M. Fang, W.J. Huang, H.B. Huang, Q.Y. Feng, M. He, J. Ji, B.Y. Liu, D.Y.C. Leung, Efficient MnOx/SiO_2@AC catalyst for ozone-catalytic oxidation of gaseous benzene at ambient temperature, Appl. Surf. Sci. 470 (2019) 439–447, https://doi.org/10.1016/j.apsusc.2018.11.146.
[35] M.C. Hu, K.S. Hui, K.N. Hui, Role of graphene in MnO_2/graphene composite for catalytic ozonation of gaseous toluene, Chem. Eng. J. 254 (2014) 237–244, https://doi.org/10.1016/j.cej.2014.05.099.
[36] J. Li, H.B. Na, X.L. Zeng, T.L. Zhu, Z.M. Liu, In situ DRIFTS investigation for the oxidation of toluene by ozone over Mn/HZSM-5, Ag/HZSM-5 and Mn-Ag/HZSM-5 catalysts, Appl. Surf. Sci. 311 (2014) 690–696, https://doi.org/10.1016/j.apsusc.2014.05.138.
[37] S.D. Li, D.D. Wang, X.F. Wu, Y.F. Chen, J. Catal, Recent advance on VOCs oxidation over layered double hydroxides derived mixed metal oxides 41 (2020) 550–560, https://doi.org/10.1016/S1872-2067(19)63446-7.
[38] Z.P. Rao, G.H. Lu, A. Mahmood, G.S. Shi, X.F. Xie, J. Sun, Deactivation and activation mechanism of TiO_2 and rGO/Er^{3+}-TiO_2 during flowing gaseous VOCs photodegradation, Appl. Catal. B 284 (2021), 119813, https://doi.org/10.1016/j.apcatb.2020.119813.
[39] F. Dong, W.G. Han, Y. Guo, W.L. Han, Z.C. Tang, $CeCoO_x$-MNS catalyst derived from three-dimensional mesh nanosheet Co-based metal–organic frameworks for highly efficient catalytic combustion of VOCs, Chem. Eng. J. 405 (2021), 126948, https://doi.org/10.1016/j.cej.2020.126948.
[40] E. Hisahiro, T. Yasutake, O. Atsushi, Catalytic oxidation of benzene by ozone over manganese oxides supported on USY zeolite, J. Catal. 305 (2013) 227–237, https://doi.org/10.1016/j.jcat.2013.05.016.